

EFFECT OF MATRIX DUCTILITY ON THE PERFORMANCE OF REINFORCED ECC COLUMN MEMBERS UNDER REVERSED CYCLIC LOADING CONDITIONS

Gregor Fischer¹, Hiroshi Fukuyama² and Victor Li³

ABSTRACT: In this paper, a research study is presented focusing on the effect of substituting brittle concrete in conventional reinforced concrete column members with a ductile engineered cementitious composite (ECC). Based on the material properties of ECC, the interaction with structural reinforcement is characterized by compatible deformations of the reinforcement and ECC matrix in the elastic and inelastic deformation regime. This unique composite deformation mechanism has significant implications on the performance of reinforced ECC structural composite members under reversed cyclic loading conditions. Important findings of this study include the extremely ductile response of steel reinforced ECC members at a simultaneous reduction of transverse reinforcement requirements as well as reduced structural damage after experiencing relatively large deformation reversals. Furthermore, the combination of ECC with structural FRP reinforcement results in composite members with an elastic load-deformation response and small residual displacements.

KEYWORDS: ECC, structural composite, reinforced concrete, FRP reinforcement, ductility, damage tolerance

1 INTRODUCTION

The ductility of conventional reinforced concrete columns is largely dependent on the amount and configuration of transverse steel reinforcement, which directly influences the effective stress-strain behavior of the confined concrete core [1], provides resistance to member shear forces, and prevents bond splitting failure as well as buckling of longitudinal reinforcement after spalling of the concrete cover [2]. Thus, transverse reinforcement effectively compensates the brittleness of concrete and indirectly provides structural ductility by assuring inelastic deformations in the longitudinal reinforcement and resisting adverse, premature failure modes.

Engineered cementitious composites (ECC) are inherently ductile and have shown to considerably improve the performance of flexural members reinforced with steel [3] and FRP reinforcement [4] under reversed cyclic loading conditions. Previous investigations on the effect of substituting concrete with ECC were conducted on small-scale specimens and revealed enhanced energy dissipation capacity and controlled damage evolution in steel reinforced ECC flexural members as well as relatively large deflection capacity and small residual displacements of FRP reinforced ECC flexural members. Furthermore, transverse

¹ Department of Civil and Environmental Engineering, University of Hawaii, USA, PhD

² Department of Structural Engineering, Building Research Institute, Tsukuba, Japan, Dr.E.

³ Department of Civil and Environmental Engineering, University of Michigan, USA, PhD

steel reinforcement at given loading configuration and specimen geometry was found ineffective and redundant in order to resist shear, buckling of longitudinal reinforcement, and provide confinement particularly at plastic hinge locations.

The research activities described in this paper are intended to verify these findings under more realistic loading conditions and larger specimen dimensions. More specifically, the effect of axial loading on the flexural load-deformation behavior is experimentally investigated using specimens at approximately one-third scale. The performance of reinforced ECC structural composites with either steel or FRP reinforcement is assessed with respect to the load-deformation behavior, energy dissipation capacity and damage evolution, failure mode, and transverse reinforcement requirements.

2 MATERIALS

The ECC matrix used in this particular study utilized 2%-Vol. Polyvinyl alcohol (PVA) fibers, cement, lime stone powder, fly ash, water, superplasticizer, and admixtures to enhance the fresh properties of the mix. Material properties in uniaxial tension obtained from this composition were a first cracking strength of 1.5MPa at 0.01% strain and ultimate tensile strength of 2.0MPa at approximately 1% strain.

In compression, the particular version of ECC used in this experimental investigation has a significantly lower modulus of elasticity compared to concrete due to the lack of large aggregates and attains its compressive strength at larger strain (Fig.1). Beyond reaching its compressive strength, the stress gradually descends, resulting in a rather ductile mode of compressive failure. In order to provide a common basis for comparison, the compressive

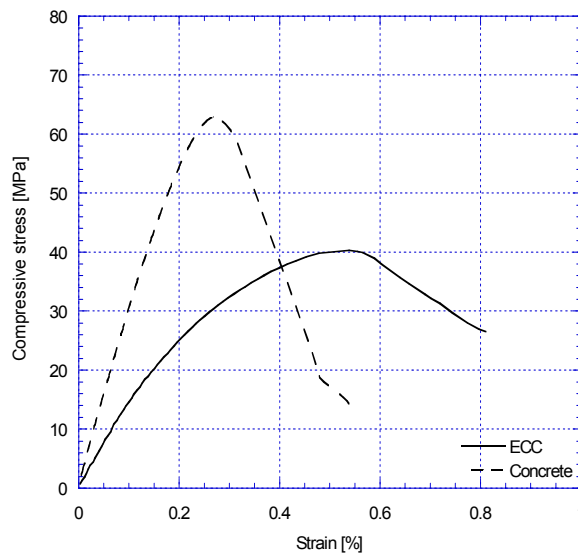


Figure 1 Stress-strain curve of ECC and concrete in compression

strength of concrete used in this study was initially chosen similar to the expected compressive strength of this version of ECC (60MPa). The compressive strength of ECC at time of testing was approximately 40MPa, which was unexpected and considerably lower than that of concrete used in the control specimens.

Concrete utilized coarse aggregates (maximum grain size 20mm), cement, water, and superplasticizer to enhance the fresh properties of the mix. Tensile tests on concrete showed tensile cracking strength of 2MPa at 0.01% strain and subsequent brittle failure. The compressive strength of concrete used in this study was approximately 63MPa (Fig.1).

For the longitudinal reinforcement of the column specimens, three types of reinforcing bars were used. The specimens with steel reinforcement were provided with deformed rebars of 13mm diameter with a yield strength of 380MPa at 0.203% strain and ultimate tensile strength of 480MPa as well as bars of 6mm diameter for longitudinal and transverse reinforcement with a yield strength of 290MPa at 0.15% strain and ultimate strength of 500MPa. Both types of reinforcing bars had an elastic modulus of approximately 190GPa.

The specimens with FRP reinforcement were provided with Carbon fiber reinforced tendons with a nominal diameter of 17.8mm (effective \varnothing 14mm), elastic modulus of 130GPa and ultimate strength of 1800MPa at 1.6% strain.

3 EXPERIMENTAL PROGRAM

3.1 DESIGN AND LOADING CONCEPT

In order to maintain a common basis for comparison of the load-deformation behavior of the composite systems considered in this study, all specimens were designed to have the same flexural stiffness in the elastic deformation regime. The amount and arrangement of the longitudinal reinforcement were determined from sectional moment-curvature analysis taking into consideration the anticipated elastic modulus of the cementitious matrices as well as that of the reinforcement materials. Assuming roughly similar elastic stiffness of the cementitious matrices, the lower elastic modulus of the C-FRP reinforcement (130GPa) as compared to steel (190GPa) had to be compensated by an inversely proportional increase in FRP reinforcement ratio.

The expected shear forces were initially determined for the steel reinforced specimens taking into consideration the nominal flexural capacity of member. Consequently, the steel reinforced concrete specimen was provided with transverse reinforcing bars in form of steel hoops in order to cover the anticipated shear demand, provide confinement of the concrete core, and prevent buckling of the longitudinal reinforcement. In the steel reinforced ECC specimen, the available shear resistance of ECC was assumed equal to its tensile strength (2.0MPa), which exceeded the expected shear demand on the column member and consequently, transverse steel reinforcement was not provided.

For FRP reinforced flexural members, the expected maximum shear forces cannot be determined by the above described procedure due to the elastic nature of the longitudinal FRP reinforcement. For the purpose of comparison it was decided to provide the same transverse reinforcement detailing in the FRP reinforced concrete and ECC specimens as in their respective steel reinforced counterparts.

The specimens were subjected to reversed cyclic lateral loading applied according to a displacement controlled loading sequence. Lateral displacements were increased incrementally up to 6% drift, beyond which, if applicable, the specimen was loaded monotonically to failure. In order to remain below the balance point of the column specimens, the axial load was kept constant at 15% of the respective compressive capacity of the specimen cross-section.

3.2 SPECIMEN CONFIGURATION AND TEST SETUP

The behavior of reinforced ECC members under reversed cyclic loading conditions was experimentally investigated and contrasted to reinforced concrete using column specimens with 1400mm height and square cross-sectional dimensions of 240mm (Fig.2). The specimens were horizontally loaded in a cantilever mode at 1200mm from the column base, which was founded on a relatively stiff transverse beam. The specimen was anchored through the transverse beam with two post-tensioned steel rods to an L-shaped testing frame, which itself was supported on a swivel mechanism in order to eliminate eccentricity effects from the axial load applied through a pin connection on top of the cantilever. The lateral load was applied to the specimen through a hydraulic actuator within the loading frame to create a self-contained, internal force flow.

In this paper, results from tests on four different composite systems are presented, specifically a steel reinforced concrete column (S-1), an FRP reinforced concrete column (S-2), a steel reinforced ECC column (S-3), and an FRP reinforced ECC column (S-4).

Specimen S-1 (steel/concrete) was longitudinally reinforced with eight D13 and four D6 rebars, symmetrically arranged in four layers within the cross-section (Fig.2). Transverse steel reinforcement (D6) was placed at 50mm spacing in the joint region and at the column base ($h=400\text{mm}$), at 100mm spacing between 400mm and 1100mm column height, and at 50mm spacing above 1100mm to prevent possible damage at the top of the specimen due to the application of axial and horizontal loading.

Specimen S-2 (FRP/concrete) was longitudinally reinforced with twelve C-FRP tendons with a nominal diameter of 17.8mm (effective 14mm) symmetrically arranged in four layers within the cross-section (Fig.2). Except the type and diameter of the longitudinal reinforcement, the arrangement of the longitudinal and transverse reinforcement was identical to specimen S-1 (steel/concrete).

Specimen S-3 (steel/ECC) had longitudinal reinforcement identical to specimen S-1 (steel/concrete), however, transverse steel reinforcement was not provided between the column base and 1100mm height (Fig.2).

Similarly, specimen S-4 (FRP/ECC) had longitudinal reinforcement identical to specimen S-2 (FRP/concrete), however, transverse reinforcement was not provided between the column base and 1100mm height (Fig.2).

Details of the specimen configurations including their expected and experimentally obtained flexural strength are summarized in Table 1.

Table 1 Summary of specimen configurations

Specimen	Composite	Axial load	Reinforcement ratio		Yielding		Ultimate	
			$\rho_{\text{long}}^{(1)}$	$\rho_{\text{trans}}^{(2)}$	Predicted ⁽³⁾	Observed ⁽⁴⁾	Predicted ⁽⁵⁾	Observed ⁽⁴⁾
S-1	R/C	520kN	2.04	1.30/ 0.65	67	80	74	88
S-2	R/C	520kN	3.22	1.30/ 0.65	-	-	100	108
S-3	R/ECC	330kN	2.04	-	55	68	62	76
S-4	R/ECC	330kN	3.22	-	-	-	78	100

¹ total longitudinal reinforcement ratio [%]

² transverse reinforcement ratio [%] below $h=400\text{mm}$ / above $h=400\text{mm}$

³ predicted shear force [kN] at yielding

⁴ observed shear force [kN]

⁵ predicted shear force [kN] from moment-curvature analysis based on material properties

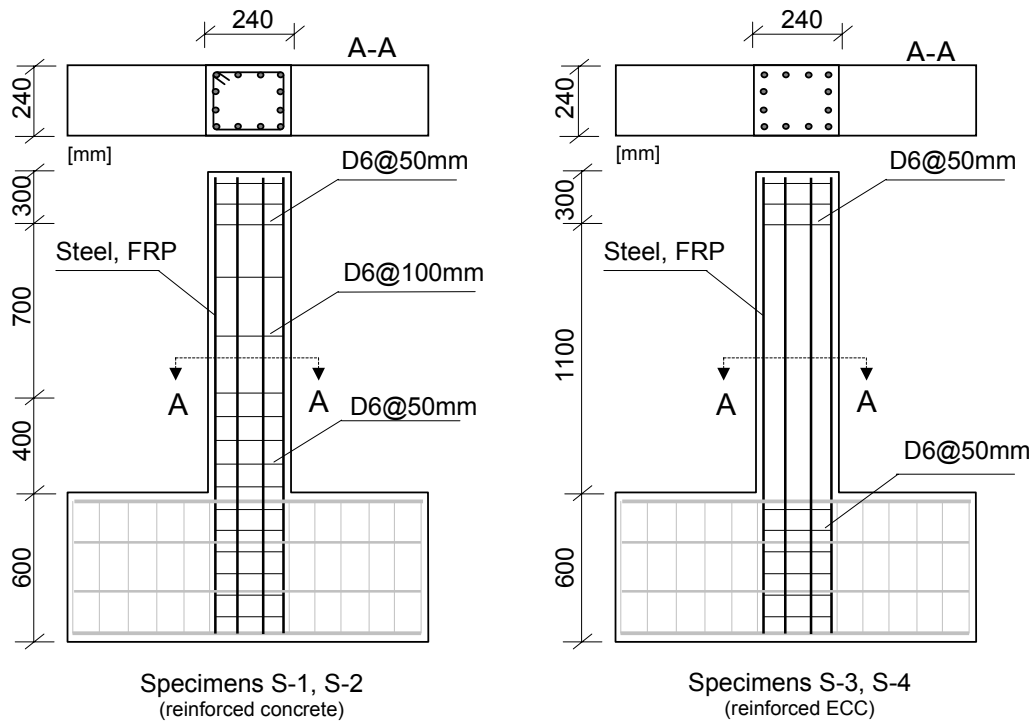


Figure 2 Specimen configurations

All specimens were instrumented with a number of measurement devices to monitor the deformation of the column at various length scales. The overall deflection of the specimen was measured with six displacement transducers spaced at 200mm distance from the column base to 1200mm height. The axial, transverse, and shear deformations of the specimen were monitored with an arrangement of transducers for each 200mm section of the column. The deformation of the reinforcement was measured with strain gages attached to one of the reinforcing bars on each side of the column at a spacing of 100mm along the entire length of the reinforcing bar.

4 TEST RESULTS AND DISCUSSION

4.1 LOAD-DEFORMATION RESPONSE AND FAILURE MODE

The response of the steel reinforced specimens (S-1, S-3) beyond formation of a plastic hinge at the column base is effectively determined by the inelastic deformation behavior of the longitudinal reinforcement in tension and the respective cementitious matrix in compression. Due to the unanticipated differences in compressive strength and modulus between concrete and ECC used in this study, the elastic stiffness and flexural strength of specimen S-1 (steel/concrete) (Fig.3a) are slightly larger than those of specimen S-3 (steel/ECC) (Fig.3b). The extensive formation of flexural cracking as well as lower elastic modulus of ECC in specimen S-3 result in a more compliant column member and consequently, the flexural stiffness of S-3 is slightly lower than that of S-1. Beyond yielding, composite damage in specimen S-1 due to bond splitting and subsequent cover spalling lead to an abrupt reduction in flexural resistance and further composite deterioration in the plastic

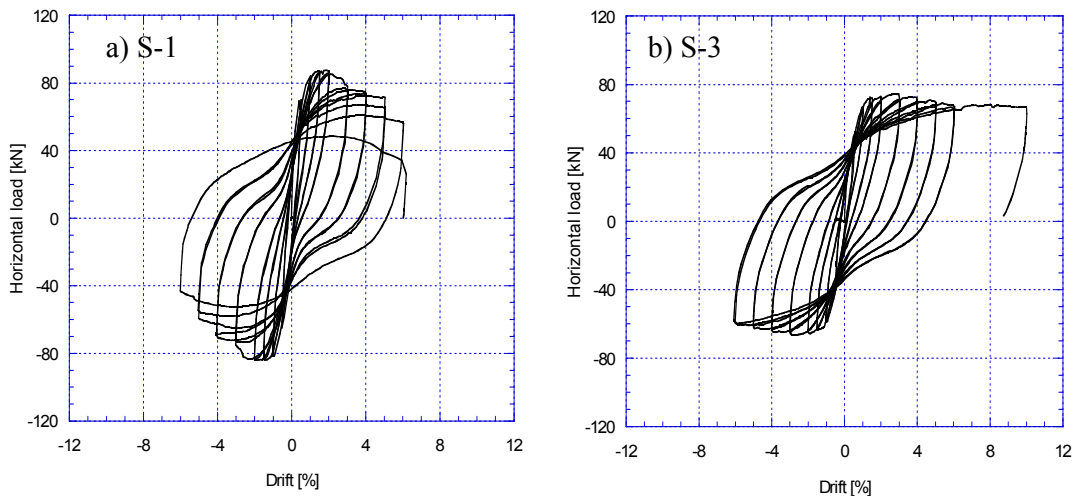


Figure 3 Load –deformation response of a) S-1 and b) S-3, both with steel reinforcement

hinge region by propagating shear cracks and crushing of the concrete core. In contrast, specimen S-3 maintains composite integrity especially at the column base and a flexural deformation mode. Compatible inelastic deformations between reinforcement and ECC reduce interfacial bond stress and bond-splitting and cover spalling are not observed. In addition, ECC provides shear resistance and confinement of the column core and the longitudinal reinforcement, which are maintained at large inelastic deformations particularly in the plastic hinge region. Consequently, composite action between steel reinforcement and ECC is preserved. At this stage, inelastic compressive deformations in ECC occur in a rather ductile mode, resulting in stable inelastic reinforcement deformations in tension and compression at load reversal. Despite crushing of ECC in the column cover and in parts of the column core, its lateral confinement effect is preserved at specimen deflections of 10% drift at essentially constant flexural resistance (Fig.3b). Throughout the entire loading procedure, specimen S-3 maintains a flexural deformation mode without shear failure.

Both specimens with FRP reinforcement show a similar load-deformation behavior up to peak load. Crack formation in specimen S-2 (FRP/concrete), however, is dominated by shear cracking, while in specimen S-4 (FRP/ECC) cracking is generally initiated by flexure. The distribution of reinforcement strain along the column height in specimen S-2 also suggests a

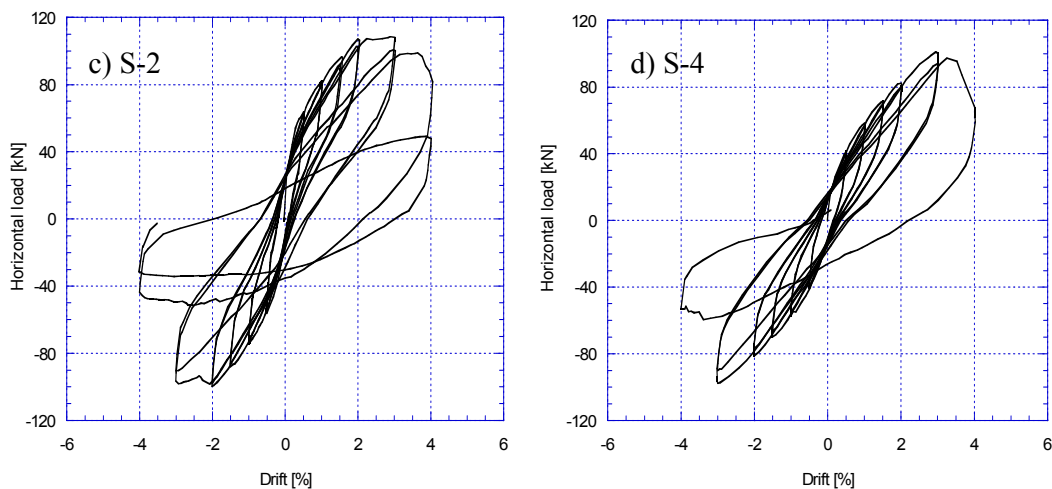


Figure 4 Load-deformation response of a) S-2 and b) S-4, both with FRP reinforcement

progressive debonding of FRP reinforcement and concrete at increasing drift levels indicated by constant strains in the FRP reinforcement between the column base and approximately 400mm height. This interfacial bond failure also propagates into the transverse beam as well as radially to the specimen surface, which is followed by concrete cover spalling in the reverse loading cycle. Failure in specimen S-2 at 3% drift is due to excessive shear and compressive stresses and subsequent concrete and FRP failure above the column base.

In contrast, reinforcement strains in specimen S-4 are decreasing with increasing distance from the column base, suggesting continuous load transfer and intact interfacial bond due to compatible deformation between elastic reinforcement and ductile ECC matrix. While the peak tensile strain in the FRP reinforcement remains well below critical (1.8% tensile strain capacity), deformations on the compression side reach levels above critical (0.2% compressive strain capacity) and induce severe damage on the FRP reinforcement, which causes rupture and subsequent failure of specimen S-4 at 4% drift.

4.2 RESIDUAL DEFLECTIONS AND ENERGY DISSIPATION

The investigation of the effect of FRP reinforcement in specimens S-2 and S-4 was motivated by an anticipated reduction of residual deflections after unloading from relatively large drift levels compared to specimens with steel reinforcement (S-1, S-3). For the purpose of evaluating the permanent deflection of the considered composite columns, a residual deflection ratio is defined herein as the residual deflection after unloading normalized by the peak deflection experienced at the respective drift level. Prior to failure of specimens S-2 and S-4, the direct comparison of the residual deflection ratio of the tested specimens (Fig.5a) clearly indicates lower residual deflections of the FRP reinforced specimens prior to failure as compared to those with steel reinforcement. However, no substantial difference between specimens S-2 (FRP/concrete) and specimen S-4 (FRP/ECC) with respect to this parameter can be derived.

In order to evaluate the energy dissipation capacity of a structural composite system, various energy dissipation mechanisms must be considered. Energy dissipation can be classified into intended, stable damage by yielding of steel reinforcement and undesirable damage due to matrix failure in compression or shear. The ability of a structural member to undergo inelastic deformation is commonly expressed by the displacement ductility factor,

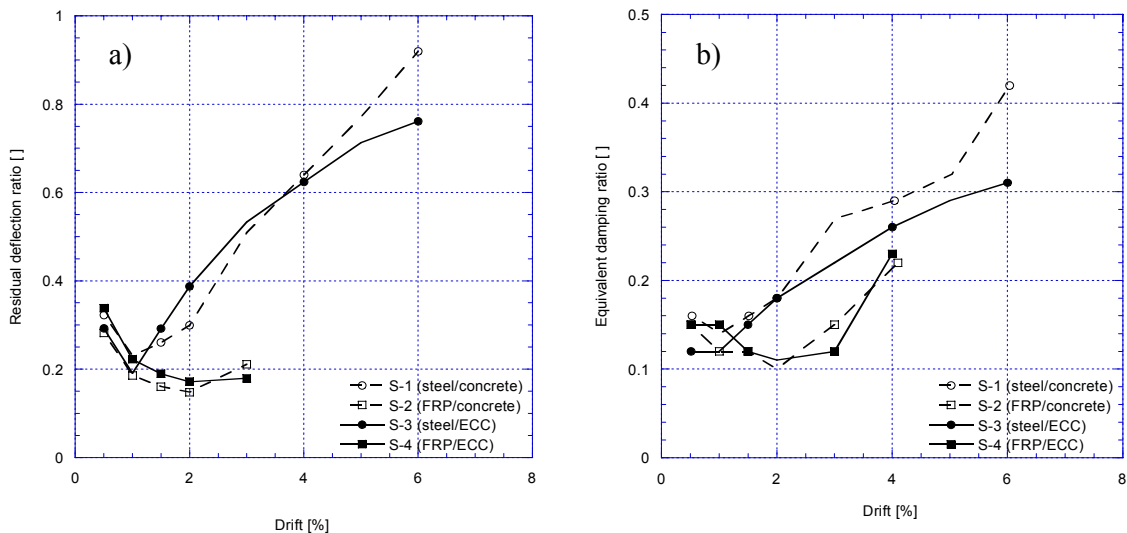


Figure 5 Comparison of a) Residual deflection ratio and b) Equivalent damping ratio

defined as the ratio between specimen deflection at 85% of the peak load and deflection at yielding of the tensile reinforcement. Based on respective specimen deflections at yield, as indicated by strain gage readings in the longitudinal reinforcement and deflections at 85% of peak load, specimen S-1 shows a ductility factor of 4 while specimen S-3 shows a factor of >10.

The equivalent damping ratio [5] characterizes the inelastic deformation behavior in more detail (Fig.5b) and can also be applied to specimens S-2 and S-4 with FRP reinforcement. In order to assess the effect of matrix cracking and tensile strain hardening of ECC in contrast to brittle deformation of concrete on energy dissipation, the equivalent damping ratio is derived from the initial loading cycle at each target drift level. Prior to reinforcement yielding in S-1 and S-3, the difference between initial and reloading cycle is sizeable, however, is found negligible beyond yielding of steel reinforcement.

Similar to the residual displacement ratio, the direct comparison of all specimens shows two basic trends depending on the type of reinforcement material. At small drift levels prior to yielding, the equivalent damping ratio in specimen S-1 (steel/concrete) is slightly larger than that of S-3 (steel/ECC), indicating that despite the ductile deformation behavior of ECC in tension, its direct contribution to member energy dissipation is similar to that of brittle concrete and negligible. This finding confirms conclusions drawn from previous tests on small-scale R/ECC and R/C specimens.

At increasing drift levels, the equivalent damping ratio remains constant or marginally decreases due to the reduced contribution of crack formation at reloading compared to that in the initial loading cycle. At yielding of steel reinforcement in specimens S-1 and S-3, the equivalent damping ratio increases at increasing drift levels, while in specimens S-2 and S-4 it remains nearly constant. Incidents of occurring damage due to concrete cover spalling, compression or shear failure become apparent as abrupt changes in the equivalent damping ratio (Fig.5b). Despite a larger ductility factor of specimen S-3 (steel/ECC) compared to S-1 (steel/concrete), the quantitative comparison of their equivalent damping ratio gives the impression of better performance of specimen S-1 compared to specimen S-3 with respect to energy dissipation. Similarly, the comparison of the total energy dissipated at each drift level leads to the same conclusion.

It is apparent from these contradicting indications, that a classification of intended and detrimental damage as well as quantitative distinction between the obvious qualitative differences in the composite deformation behavior and damage state especially of specimens S-1 and S-3 cannot be conclusively derived from the above parameters.

4.3 TRANSVERSE REINFORCEMENT REQUIREMENTS

The objective of comparing the reinforced concrete columns with transverse steel reinforcement (S-1, S-2) to the reinforced ECC columns without transverse steel reinforcement (S-3, S-4) is to assess the shear capacity of reinforced ECC members at given specimen geometry. Previous experimental investigations on small-scale specimens indicated a redundancy of transverse steel reinforcement in steel and FRP reinforced ECC members due to predominant flexural crack formation and resulting orientation of stirrups parallel to the flexural crack planes.

Specimens S-1 (steel/concrete) and S-3 (steel/ECC) both experience a flexural failure mode, i.e. yielding of longitudinal steel reinforcement at sufficient shear resistance provided by the stirrups in specimen S-1 and by ECC in specimen S-3. The shear strain distributions of both specimens at 3% drift (Fig.6a) indicate that shear distortions primarily occur in the plastic hinge region. Furthermore, the relative magnitude of shear strain in the plastic hinge

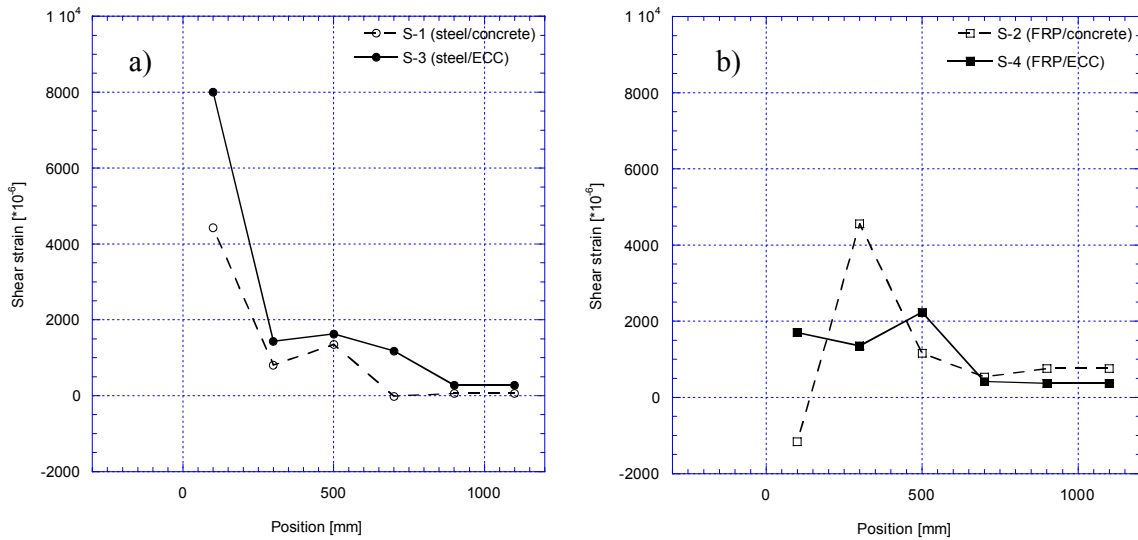


Figure 6 Comparison of shear strain distribution in a) S-1, S-3 and b) S-2, S-4

region indicates that specimen S-3 has a lower shear stiffness relative to specimen S-1. Shear distortions in S-3 occur between the column base and approximately 700mm height, which roughly outlines the extent of flexural crack formation and suggests that shear strains originate from horizontal sliding along interconnected flexural crack planes due to the lack of sufficient aggregate interlock. Shear distortions in specimen S-1 also occur primarily between the column base and 500mm height, outlining the extent of shear crack formation along the specimen height.

The distribution of shear strain in the specimen S-4 (FRP/ECC) at 3% drift (Fig.6b) is rather uniform between the column base and 700mm height and well below the values observed in specimen S-3 (steel/ECC), possibly due to smaller flexural crack widths and more uniform shear stiffness along the specimen height. The relatively small magnitude of shear strain at 3% drift confirms experimental observations that failure of specimen S-4 at 4% drift is not initiated by insufficient shear capacity.

The shear strain distribution in specimen S-2 (steel/concrete) appears somewhat counterintuitive, since strains at the column base are negative while sections above 200mm height show positive shear strains. The deformation measurements at the column base are possibly affected by severe damage experienced in specimen S-2 particularly at this section.

5 CONCLUSIONS

The structural performance of steel reinforced ECC flexural members is characterized by relatively stable inelastic load-deformation behavior and large deflection capacity. In comparison to reinforced concrete, the ductile deformation behavior of ECC has significant effect on the composite integrity particularly in the plastic hinge region and therefore the structural composite maintains stable inelastic deformations of the steel reinforcement, i.e. ECC assists stable steel yielding in order to utilize its energy dissipation capacity to a maximum extent. However, the direct contribution of ECC to energy dissipation is negligible. The resistance to shear in reinforced ECC is entirely provided by the inherent shear capacity of ECC and does not require transverse steel reinforcement.

While the response of steel reinforced concrete and ECC specimens is similar to that observed in previously tested small-scale specimens, FRP reinforced members investigated in this study were found highly sensitive to compressive deformations in the cementitious matrix. Prior to failure, FRP reinforced ECC showed elastic load-deformation response and stable flexural crack formation. However, excessive compressive strain on the FRP reinforcement lead to failure at relatively small column deflections similar to those observed in FRP reinforced concrete. These findings are in contrast to those derived from small-scale tests on FRP reinforced ECC flexural members, which showed deflection capacity of approximately 7% drift in case of CFRP longitudinal reinforcement.

The relatively low stiffness of ECC results in a rather ductile failure mode in compression and consequently in improved deflection capacity of steel reinforced ECC members. However, for FRP reinforced ECC members the elastic modulus of the cementitious matrix must be significantly increased in order to avoid large compressive strain and damage in the longitudinal FRP reinforcement.

ACKNOWLEDGEMENT

The research activities described in this paper have been supported by a grant from the National Science Foundation (CMS-0070035) to the ACE-MRL at the University of Michigan and by the Building Research Institute, Tsukuba, Japan. This support is gratefully acknowledged. In particular, the authors would like to thank Mr. M. Iso and Mr. H. Suwada for their significant contribution to this research project.

REFERENCES

- Ahmad, S.H., Shah, S.P. (1982), "Stress-Strain Curves of Concrete Confined by Spiral Reinforcement", *ACI Journal*, Vol. 79, November-December 1982, pp. 484-490
- Chopra, A.K. (1995), "Dynamics of Structures – Theory and applications to Earthquake Engineering", Prentice-Hall, Inc.
- Fischer, G., Li, V.C., (2001a), "Deformation behavior of FRP reinforced ECC flexural members under reversed cyclic loading conditions", submitted to *ACI Structural Journal*
- Fischer, G., Li, V.C., (2001b), "Effect of matrix ductility on deformation behavior of steel reinforced ECC flexural members under reversed cyclic loading conditions", submitted to *ACI Structural Journal*
- Watson, S., Zahn, F.A., Park, R. (1994), "Confining Reinforcement for Concrete Columns", *ASCE Journal of Structural Engineering*, Vol. 120, No.6, pp.1798-1823